

Neutron and γ -ray Discrimination by a Pressurized Helium-4 Based Scintillation Detector

Shubham Dutta^{a,*}, Sayan Ghosh^c, Satyajit Saha^b

^a*High Energy Nuclear and Particle Physics Division, Saha Institute of Nuclear Physics - a CI of Homi Bhabha National Institute, Block AF, Sector I, Bidhannagar, Kolkata, 700064, , India*

^b*Applied Nuclear Physics Division, Saha Institute of Nuclear Physics - a CI of Homi Bhabha National Institute, Block AF, Sector I, Bidhannagar, Kolkata, 700064, , India*

^c*Department of Physics and Astronomy, Purdue University, West Lafayette, 47907, IN, USA*

Abstract

Pressurized helium-4 based fast neutron scintillation detector offers an useful alternative to organic liquid-based scintillator due to its relatively low response to the γ -rays compared to the latter type of scintillator. In the present work, we have investigated the capabilities of a pressurized ^4He (PHe) detector for the detection of fast neutrons in a mixed radiation field where both the neutrons and the γ -rays are present. Discrimination between neutrons and γ -rays is achieved by using fast-slow charge integration method. We have also conducted systematic studies of the attenuation of fast neutrons and γ -rays by high-density polyethylene (HDPE). These studies are further corroborated by simulation analyses conducted using GEANT4, which show qualitative agreement with the experimental results. Additionally, the simulation provides detailed insights into the interactions of the radiation quanta with the PHe detector. Estimates of the scintillation signal yield are made based on our GEANT4 simulation results by considering the scintillation mechanism in the PHe gas.

Keywords: Pressurized helium-4 detector, neutron - gamma discrimination, neutron spectroscopy, neutron attenuation, GEANT4 simulation

1. Introduction

Neutrons as radiation quanta, are found in nature because of their release in various forms of nuclear reactions, most common being the nuclear fission and the

*Corresponding author

Email address: shubhamdutta_16@yahoo.com (Shubham Dutta)

(α, n) reactions caused by the natural radioactivity of the remnants of Uranium-Thorium (U-Th) decay chain. Free neutrons are, however, unstable against β -decay with about 15 minutes of half life. In spite of this fact, free neutrons pass and penetrate through matter since they are charge neutral and deposits partial or full energy through hadronic interactions. These interactions include capture into nuclei and elastic scattering, resulting in nuclear recoil of the stopping media. Such interactions take place over a very short time scale compared to the half-life of free neutrons, which make it possible to detect them in real life.

Neutrons are produced in large number inside the core of the nuclear reactors and also emerge out of the spent nuclear fuels by spontaneous fission and (α, n) reactions[1]. These neutrons, detected with the help of suitable neutron detectors, are often used to monitor the spent fuel repositories and also at the strategic surveillance stations for monitoring hidden nuclear materials. In that respect, neutron detectors, capable of detecting neutrons up to around 10 MeV energy, serve the purpose. However, since the neutrons are most often found in a mixed radiation field with dominance of mostly γ -rays, X-rays and electrons coming out of the same sources, it is important to achieve discrimination between the neutrons and the other radiation quanta before any meaningful result can be extracted.

Neutron background for a typical dark matter search experiment, usually set up at underground laboratories, interferes with the signal due to possible dark matter candidates, as both the radiation quanta interact with active media to produce overlapping signals. These neutrons are predominantly produced by the (α, n) reactions due to the U-Th decay chain products emitting α -particles. Careful measurements of the neutron background is essential at every site to assess the sensitivity limits. Pressurized helium-4 (PHe) detector has been used recently at such facilities to monitor the residual neutron flux[2].

Liquid helium[3] has been investigated as scintillator for neutron detection more than 60 years back. However, the scintillation properties of PHe gas have been examined much later for successful implementation as fast neutron detector[4]. The major advantage of PHe gas as scintillator is its relatively weak response to β -particles and γ -rays, because the density of available electrons in helium is much less than in standard scintillators, organic and inorganic. On the other hand, neutrons cause nuclear recoil of the helium-4 nuclei inside the pressurized gas, resulting in multiple processes of ionization and other interactions, leading to scintillation through transitions from the singlet excimer states or the triplet excimer states[5]. Both the transitions lead to emission in the extreme ultraviolet (EUV) region of the electromagnetic spectrum, with wavelength of maximum emission around 80 nm. A wavelength shifting (WLS) compound is used to make the EUV scintillation light output readable by

photomultipliers (PMTs) or silicon photomultipliers (SiPMs)[6, 7].

In recent times, PHe detectors are made commercially available by Arktis Radiation Detectors Ltd, Switzerland[8]. Front-end electronics and data acquisition system is provided as a package for measuring the fast and the thermal neutron fluxes after pulse shape discrimination using Time-over-Threshold (ToT) technique to discriminate between γ -rays, fast neutrons and the thermal neutrons. The inner wall of the detector is coated with a Lithium-based compound to make the detector sensitive to the thermal neutrons. These neutrons undergo capture by Lithium to produce energetic α -particles which result in scintillation inside the detector volume. Corresponding ToT signals are found to be larger than those produced by the fast neutrons. Some technical details about the variant detector model S670, which is not sensitive to the thermal neutrons, can be found elsewhere[9].

Aim of this work is the following: 1) discrimination of fast neutrons from the γ -rays and electrons using fast-slow charge integration method; 2) qualitative study of attenuation of the fast neutrons and γ -rays by high density polyethylene (HDPE); 3) estimation of threshold for neutron and γ -ray discrimination; 4) carry out a detailed simulation to understand the interaction of the neutrons and γ -rays with the PHe media; 5) follow the systematics of energy transfer from the neutrons and the γ -rays to ^4He (nuclear recoil) and electrons (electron recoil) respectively; and 6) to estimate the resulting scintillation signals following excitation and charge transfer collision processes in the PHe.

2. Experimental details

2.1. Instrumentation

A photograph of the experimental set up is shown in the Fig. 1a. Arktis-made PHe detector and a radioactive source (^{252}Cf source inside a PTFE capsule), placed in front of the detector, are displayed in the photograph. The active medium of the detector is ^4He gas at a pressure of 150 - 180 bar, enclosed inside a stainless steel tube of 60 mm inner diameter and 600 mm active length. Details about the detector, related electronics and their working principles are given in many references available as published articles[6, 10]. The detector is packaged with SiPM arrays as photon readout located inside the pressurized detector volume. The detector is segmented into three parts along the length of the cylindrical tube. Photons from each segment are read out by an array of 8 SiPMs. Signals from two SiPMs are summed and fed into each output, so that 4 output signal pulses are generated from each segment.

For our work, the digital electronics readout system was replaced by a multichannel analog circuit (provided by the manufacturer) for analog signal processing using

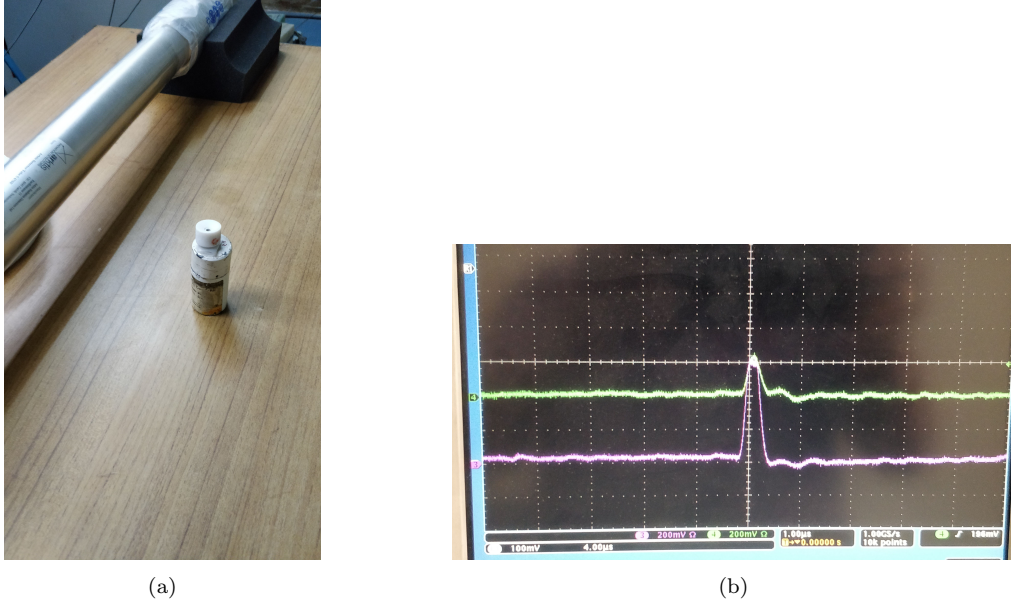


Figure 1: (a) Experimental set up involving Arktis detector and ^{252}Cf source inside teflon capsule; (b) signal traces of the amplified pulses from the detector.

conventional electronics and a 12-bit current integrating analog to digital converter or QDC (16 channel Phillips Scientific charge ADC, Model 7187). The pulses from the SiPMs are fed to the analog circuit, which consists of a preamplifier and a shaping amplifier with baseline restorer for each SiPM channel. Traces of the output pulses from the amplifier are shown in the Fig. 1b. The output signals were inverted using high speed pulse transformer (ALT 4532M) to match with the polarity and pulse timing requirements. Out of the four output signals from a segment, one signal was fed to a low threshold discriminator to generate the logic gates for the QDCs required for pulse shape discrimination (PSD) between neutrons and γ -rays or electrons. The PSD parameter (P) is defined as: $P = NQ_S/(Q_S + Q_L)$ where, Q_S and Q_L are the charge contents of the pulse within the duration of the short gate and the long gate respectively and N is a scaling factor to convert the ratios to suitable integer values for the plots.

2.2. Measurements with Radioactive sources

The systematic studies were done using different neutron and γ -ray sources placed at a certain distance from the detector as shown in the photograph (see Fig. 1a). Provision for placement of different absorber materials in between for systematic studies was also made. An unmoderated ^{252}Cf spontaneous fission source (half-

life = 2.645 years, spontaneous fission branching ratio = 3.09%[11]) was used for simultaneous detection of neutrons and γ -rays. The source emits fast neutrons with average energy of 2.12 MeV. The source, with a strength of $\sim 1 - 5$ kBq, was sealed inside a cylindrical PTFE capsule having an opening on one of the flat faces. The aperture diameter was 2 mm, which was sealed with a 100 μm thick polyethylene terephthalate (PET) window.

A typical scatter plot of the PSD parameter P vs. Q_L is shown in Fig. 2 for the ^{252}Cf source placed near the detector. Two distinct bands can be seen in the scatter plot obtained after 5 hours of exposure to the ^{252}Cf source. The relative configuration

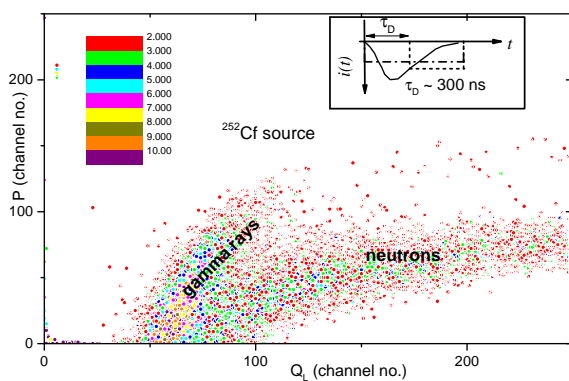


Figure 2: Scatter plot of the PSD parameter P as function of Q_L obtained by exposure of ^{252}Cf source. Inset shows the gate configurations for the short and the long gates.

of the gates, optimized by adjusting gate widths and delays by looking at P , is also shown in the Fig. 2. Optimum delay between the threshold for the up-swing of the pulse and the trigger point of the short gate was found to be around 300 nanosecond for achieving good discrimination.

A ^{137}Cs monoenergetic (662 keV) γ -ray source, with strength ~ 30 kBq, was used for the experiment to identify the γ -band as distinct from the neutron band. The scatter plot, obtained after exposing the detector with the γ -ray source, is displayed in the Fig. 3, which shows a single band (γ -band) as expected. From the scatter plot of Fig. 2, the neutron and the γ -bands are found to merge at low Q_L values, which qualitatively indicates the low energy threshold for discrimination. A comparison of projection of the neutron and the γ -bands on the Q_L axis is shown in the Fig. 4. It reveals that the detector response to the γ -rays, mediated mostly through electron recoil, is quite low compared to that for the neutrons having energies

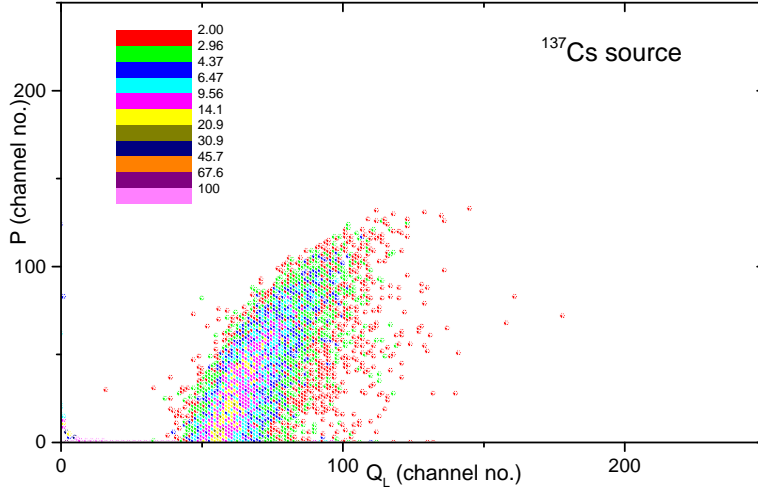


Figure 3: Scatter plot of the PSD parameter P as function of Q_L obtained by exposure of a ^{137}Cs γ -reference source.

of the same order. It can be seen from the plots that the nuclear recoil spectrum due to the neutrons terminate abruptly at higher channels ($\gtrsim 250$), which is due to the saturation of the pulses of the SiPM signal amplifiers provided by the manufacturer.

2.3. Measurements with ^{241}Am X-ray source

A ^{241}Am X-ray source, embedded in a glass matrix and sealed inside a cylindrical stainless steel capsule, was also studied with the detector. The source, having a strength of ~ 100 MBq, is originally intended for energy calibration of X-ray detectors. This source was used in the experiment to determine the response of the detector to low energy photons so that a low energy cut-off for electron recoil could be established. The scatter plot of P vs. Q_L , obtained after 5 hours of exposure, is shown in the Fig. 5a. A clear neutron band, besides the γ -band, was observed to appear. This was a bit surprising due to the reason that 1) the source was used so far for energy and relative efficiency calibration of the X-ray detectors, and 2) it was never monitored with neutron detectors or dosimeters. Surprisingly, the same exposure time (5 hours) for the ^{241}Am and the ^{252}Cf sources to the PHe detector was used.

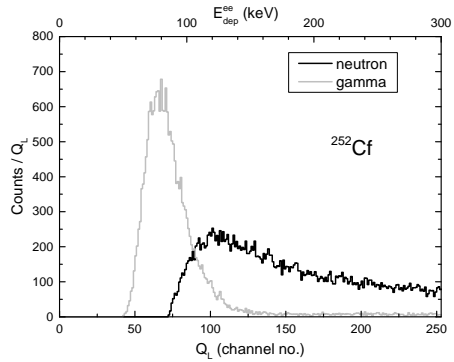


Figure 4: Projection spectra of the neutron band and the γ -band obtained by gating on the respective bands for exposure to the ^{252}Cf source.

In order to confirm that the band is due to the neutrons being detected, attenuation of the band population by high density polyethylene (HDPE) was studied. For this purpose, 4 layers of HDPE, each being 25 mm thick with a total thickness of 100 mm, were placed between the ^{241}Am source and the PHe detector to attenuate the neutrons. The scatter plot (P vs. Q_L), obtained over the same exposure time, is shown in the Fig. 5b. It clearly reveals attenuation of the neutron band. The plots,

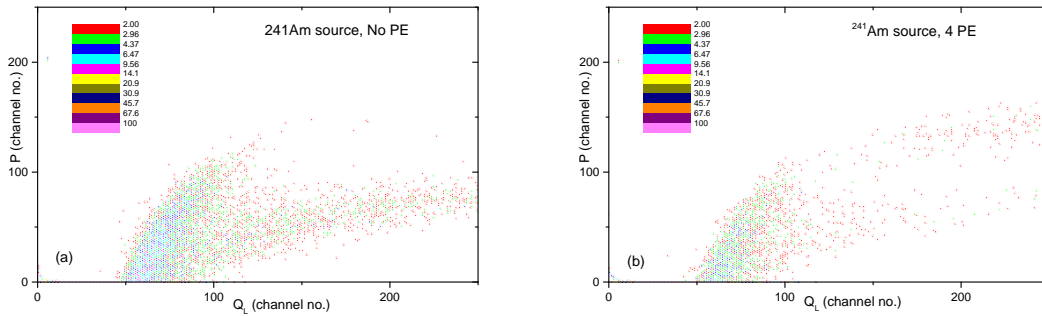


Figure 5: (a) Scatter plot of the PSD parameter P as function of Q_L obtained by exposure of a sealed ^{241}Am source; (b) same plot obtained after blocking the neutrons by 100 mm thick HDPE absorber.

obtained by gating on the neutron band and projection taken along the Q_L axis (see Fig. 6), provide a comparison of the neutron attenuation by the HDPE layers. Low energy neutrons are expected to be attenuated more than those of higher energies, however from the plot, the attenuation factor appears to be fairly independent of energy. This is due to the moderation of the energetic neutrons that enhances counts at low energy and suppresses at higher energy. Similar projection spectrum for the γ -band is shown in the Fig. 7, where attenuation of γ -rays is observed. We also have observed build-up of counts in the high energy tail (larger Q_L). This was investigated in detail through simulation in Sec. 3.4.

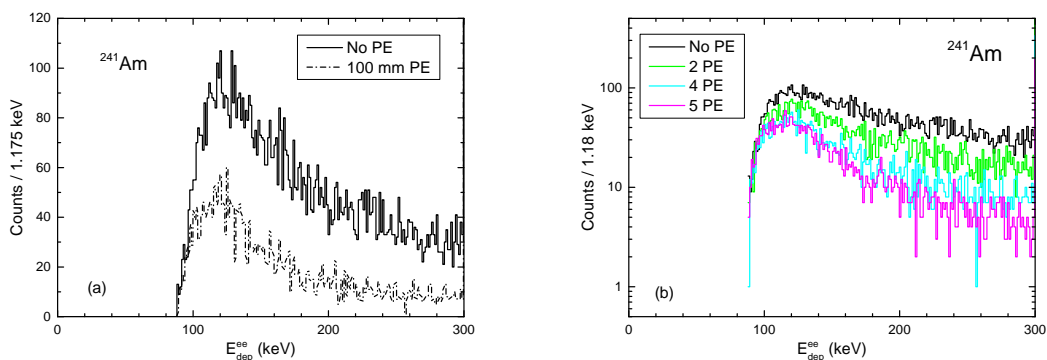


Figure 6: (a) Projected spectra on the Q_L axis after setting a banana gate on the neutron band with and without the HDPE layers between the source and the detector. Attenuation of neutrons due to HDPE is evident; (b) comparison of the projected neutron spectra recorded after the neutrons travel through different numbers of the HDPE layers. See Sec. 3.4 for the energy calibration applied here.

3. Results and analysis

3.1. Simulation

A detailed simulation of response systematic of the detector to the relevant radiation quanta (neutrons, γ -rays) were done to understand the nuclear-recoil events (NR) due to the neutrons and the electron-recoil (ER) events due to the γ -rays, and to compare them qualitatively with the results obtained from the experiment. It is evident from the previous section that the scope of simulation are 5-fold: 1) emission of relevant radiation quanta from the radioactive source used, particularly the ^{241}Am source; 2) response of the detector to the neutrons, more specifically to the fast neutrons; 3) attenuation of the fast neutrons by suitable plastic absorbers (HDPE); 4)

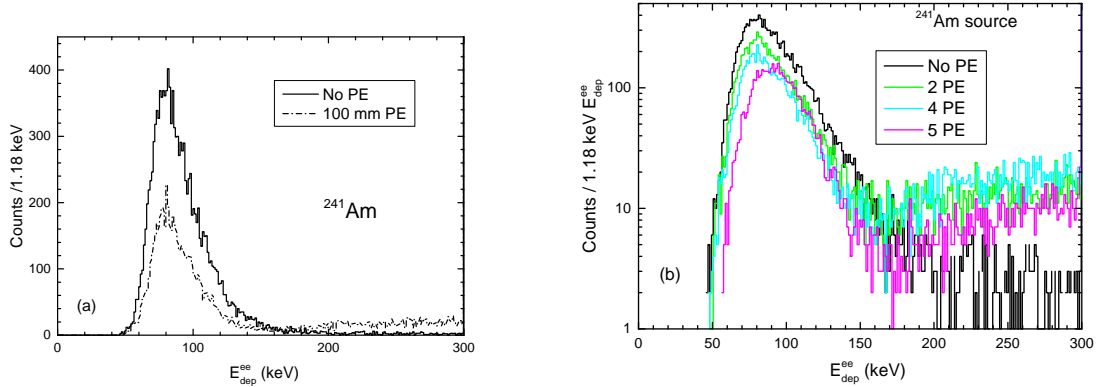


Figure 7: Same as Fig. 6 except that the banana gate is set on the γ -band. (a) projected spectra with and without the HDPE layers between the source and the detector. See Sec. 3.4 for the calibration procedure applied in the plot.(b) Comparison of the projected γ -spectra recorded after the neutrons travel through different numbers of the HDPE layers. The x -axis scale on the bottom displays the electron equivalent energy loss E_{dep}^{ee} of neutron. See Sec. 3.3 for its definition.

response of the detector to the γ -rays emitted from the radiation sources and also resulting from neutron absorption in HDPE; 5) discrimination between the neutrons and the γ -rays using signal analysis.

Simulations were carried out by the GEANT4 (G4) simulation toolkit [12], version 10.7.4. G4 provides numerous handles to tune the simulation parameters, allowing users to focus on specific aspects of interest at a time. A custom physics-list is utilized in our simulation, which is based on the one developed by Mendoza et al.[13]. We will briefly outline the G4 packages used in this physics-list to model various interactions. The G4RadioactiveDecayPhysics package is used for modeling of the radioactive decays, relevant for the ^{241}Am source. It uses the ENSDF database [14] for the various decay parameters including the energy levels of the daughter nuclei. The production of neutrons from (α, n) reaction is modeled using the G4ParticleHP package, which is capable of utilizing the ENDF-6 formatted data libraries[15]. The database used for this purpose is the JENDL/AN-2005 dataset [16]. The QGSP_BIC_HP model is used for the hadronic interactions and uses the G4 Neutron Data Library (G4NDL) to implement low energy neutron interactions with high-precision. The EM interactions are modeled with the G4EmStandardPhysics.option4 package.

The geometry to obtain the particle spectra consists of a cylindrical stainless steel source capsule of 6 mm diameter \times 9 mm length, with the ^{241}Am source, embedded

in a pyrex glass matrix of 3 mm diameter \times 6 mm thickness, placed inside and sealed with a stainless steel cover. The source capsule is surrounded by a spherical *dummy* detector, which is made of air. This is placed to track the particles that are being emitted from the source.

^{241}Am (432 years half-life) is used as the primary α -emitter nucleus embedded within the glass matrix. It decays to ^{237}Np by emitting α -particles at 5.486 MeV ($\sim 85\%$ decay branch), 5.443 MeV ($\sim 13\%$ decay branch), and the rest at other energies. Np^{237} daughter nucleus has a half life of approximately 4 orders of magnitude more than that of ^{241}Am . Therefore, the source is approximated as an alpha emitter whose energy is sampled from the spectrum as obtained from G4. These α -particles are allowed to penetrate isotropically through the base material of the source capsule, where they undergo (α, n) reaction with the constituent nuclei. Based on the cross-section data available from the database, respective elemental compositions of the materials and the relevant energies of the α -particles, we find that the dominant reaction producing neutrons are: $^{11}\text{B}(\alpha, n)^{14}\text{N}$ ($\sim 69\%$) and $^{23}\text{Na}(\alpha, n)^{26}\text{Al}$ ($\sim 11\%$), rest are being produced by various other reactions.

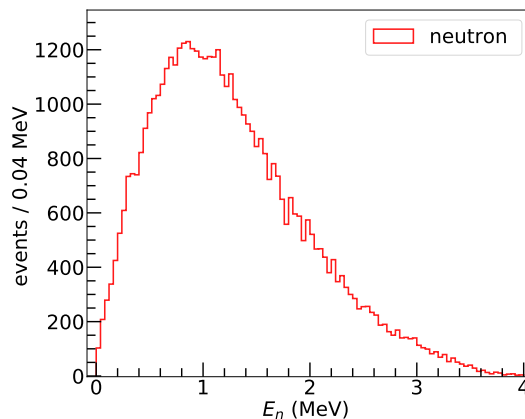


Figure 8: Simulated energy spectrum of the neutrons arising from the ^{241}Am source capsule.

The neutron yield from these (α, n) reactions is found to be very low, ~ 1 per million for the impinging α -particles. Accumulating sufficient statistics would require significant amount of computation time. The physics-list has the option to bias the (α, xn) cross-section by a fixed factor in order to increase the neutron yield. The developers of the physics-list have tested and verified that the biasing technique do not impact the neutron energy spectrum [13]. A biasing factor of 10000 was used. The resulting neutron spectral distribution is shown in the Fig. 8. The neutron spectrum has a peak at ~ 1 MeV and extends up to ~ 4 MeV.

3.2. Neutron Response Systematics by $G4$

The geometry of the PHe detector is mentioned in Sec. 2.1. For this study, the source is placed at a fixed distance from the PHe detector to accommodate the neutron absorbers (HDPE) in between. The HDPE absorber slabs, each 25 mm thick, are cumulatively placed to record the resulting neutron energy spectral distributions as seen by the PHe detector.

As mentioned in Sec. 1, neutron scatters off a ${}^4\text{He}$ nucleus transferring a part of its kinetic energy (E_n). The recoiling ${}^4\text{He}$ deposits the recoil energy within the fiducial volume of the detector via ionization, followed by scintillation. The recoiling ${}^4\text{He}$ deposits its entire energy within the volume, which is designated as E_{dep} . The E_{dep} spectra for monoenergetic neutrons at different energies ranging from 0.25 to 3 MeV are estimated as shown in the Fig. 9a. Since there is spread in the E_{dep} spectra, we have estimated the 90% value of the total area under the spectral profile. Subsequently, we have determined the upper limit of the E_{dep} parameter for the integral under the spectral profile, which matches with the above-mentioned number. We have designated the corresponding upper limit on E_{dep} as the marker (ΔE) of the corresponding recoil signal registered by the detector. A plot of (ΔE) as function of E_n is shown in the Fig. 9b. The (ΔE) is found to be fairly linear with the incident energy E_n . Therefore, from the E_{dep} spectrum, an estimate of the incident energy may be done.

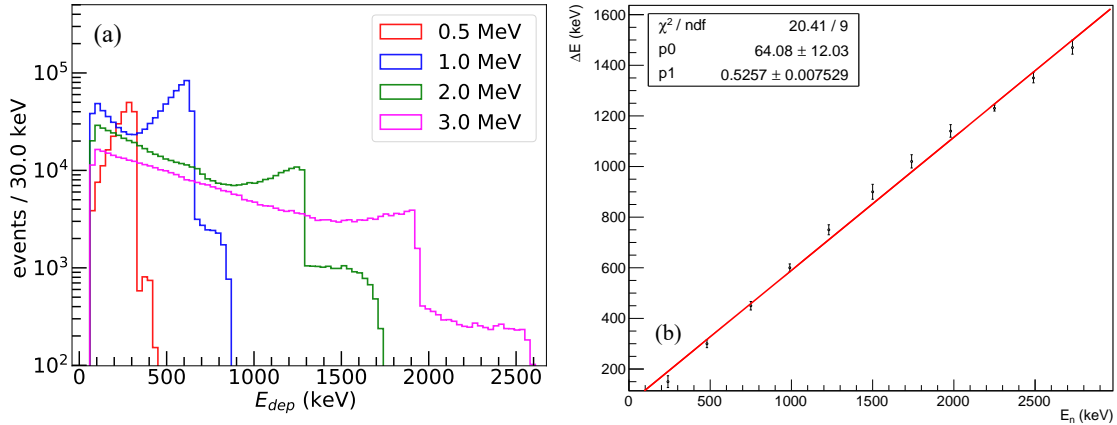


Figure 9: (a) Simulated E_{dep} spectrum of the mono-energetic neutrons; (b) ΔE is plotted against energy of the neutrons. See Sec.3.2 for the definition of the ΔE parameter.

It may be noted that the recoiling ${}^4\text{He}$ deposits its entire energy within the volume. Also, one neutron is found to cause multiple nuclear recoil during its passage. Therefore, each recoil is also recorded as a distinct event for systematic studies and

calculation of S1 signal (to be explained in Sec. 4). The HDPE slabs are cumulatively placed and the simulations are done for 50 million events for each thickness of the absorber. Only the fast neutron events selected by energy cut of $\lesssim 70$ keV, are recorded. Fig. 10a shows the distribution of the E_{dep} corresponding to the fast neutron events, which can be compared with the spectra obtained experimentally (see Fig. 6b). The relative ordering of the plots for different thicknesses of the HDPE absorbers agrees with the experiment.

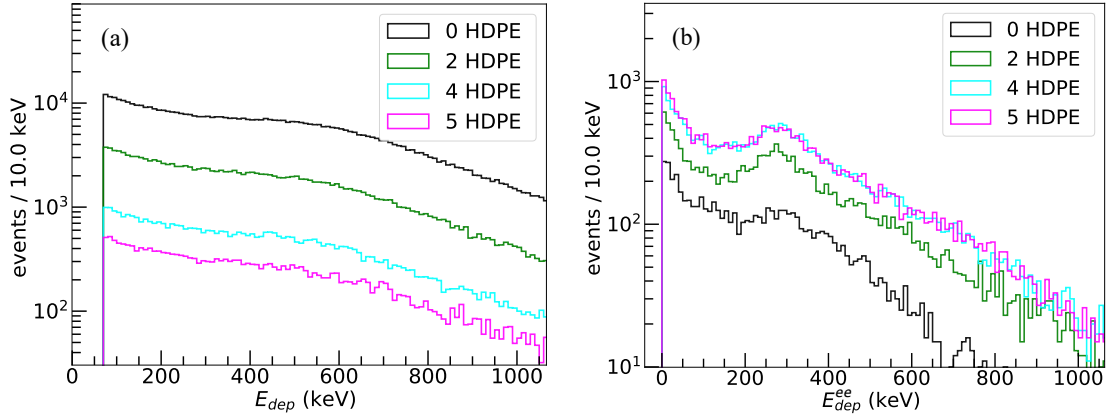


Figure 10: E_{dep} spectrum of the (a) NR events and (b) ER events from G4 simulation. In both the cases, the neutrons from the ^{241}Am source pass through the HDPE layers before falling on the detector.

3.3. Electron recoil events

γ -rays falling on the PHe detector cause electrons inside the gas to recoil and thus, result in electron recoil signal. This is demonstrated in our experiment (see Fig. 3) with ^{137}Cs standard γ -ray source as well. The range of E_{dep} values can be seen to merge with the lower range of E_{dep} values for the neutrons as shown in the Fig. 4, where the spectra for the neutrons and the γ -rays from ^{252}Cf are overlaid.

It has already been demonstrated by exposing the detector with ^{241}Am source that the neutrons are attenuated by the HDPE layers (see Sec. 2.3). It is also shown that while the γ -ray spectrum at the lower channels along the x -axis get significantly attenuated (see Fig. 7) after passing through the HDPE layers, the higher channels corresponding the larger E_{dep} values get populated as well. For measurements with different number of HDPE layers in between, we observe that after traversing two HDPE layers, the spectrum at the higher channels (i.e, region of interest or RoI > 150) show a rising trend and a bump around 240 channel number till it reaches

saturation at the highest channel. There is not much visible relative change for four HDPE layers. However, the spectral population over the RoI diminish after passing through five HDPE layers. This may be interpreted as due to the production of 2.225 MeV γ -rays from neutron moderation within the HDPE, followed by absorption in HDPE through the $n + p = d + \gamma$ process. A simulation of the γ -ray interaction with the detector is done to understand the origin, the nature of the γ -ray spectra and the underlying systematics of the process.

The γ rays falling on the detector will produce electron recoil within the pressurized ^4He -volume. The study is more complicated due to the presence of stainless steel housing of the detector which contains high Z elements. Since the γ -rays are energetic to undergo pair creation, positrons are also produced, which result in the production of 511 keV γ -rays. Therefore, the electron-recoil events, though largely contain effects due to the electrons, there would be effect due to the positrons as well. Fig. 10b includes the energy loss spectra for the electron recoil events, when the neutrons emitted from the ^{241}Am source, are incident on the detector. Henceforth, we will designate the energy loss by the electrons as E_{dep}^{ee} to distinguish it from E_{dep} due to the neutrons.

3.4. Gamma-ray Response Systematics by G4

In the simulation procedure, mono-energetic γ -rays of different energies (E_γ) are allowed to impinge upon the detector. The E_{dep}^{ee} spectrum of the recoiling electrons is shown in Fig. 11a. A peak begins to appear at $E_{dep}^{ee} \sim 280$ keV as the energy of the incident γ -ray is increased. The γ -ray energy threshold for appearance of the peak is found to be around 650 keV. Therefore, the 847 keV γ -ray, which arises from the $^{56}\text{Fe}(n, n'\gamma)$ reaction, would also give rise to the ~ 280 keV peak due to the presence of SS housing, when no HDPE slab is placed. A detailed event-by-event tracking reveals that this number corresponds to the most probable E_{dep}^{ee} of the recoiling electrons given the geometry (diameter) of the detector. The ΔE values for the E_{dep}^{ee} spectra as function of E_γ is plotted in the Fig. 11b, which indicates saturating trend at higher energies. The contour is fitted with a quadratic function, modulated by a smooth step function of the form:

$$F(x) = 0.5 \cdot (1 - \tanh((x - p0)/p1)) \cdot (p5 \cdot x^2 + p3 \cdot x + p2) + 0.5 \cdot p4 \cdot (1 + \tanh((x - p0)/p1))$$

where, $p0$ to $p4$ are the parameters for the fit. The step-function makes the quadratic term dominant in the low E_γ region and the constant term (saturation value) dominant in the high E_γ region. Specifically, $p0$ marks the threshold when the saturation begins dominating, while $p4$ denotes the saturation value.

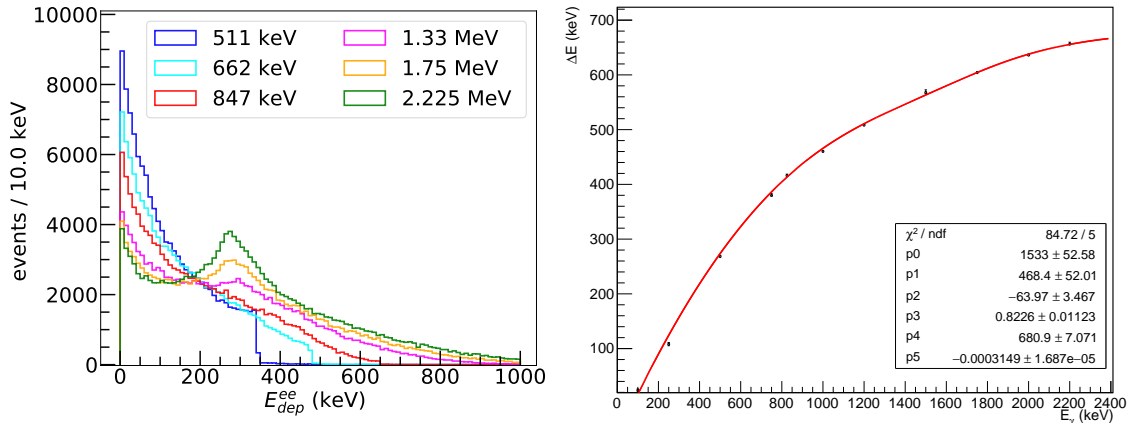


Figure 11: (a) E_{dep}^{ee} spectrum of mono-energetic γ -rays, and (b) corresponding 90% contour values are plotted as function of the γ -ray energy.

The saturating behaviour in the Fig. 11b arises due to the fact that the recoiling electrons do not lose their entire energy within the detector. This can be seen more explicitly in Fig. 12, where the E_{dep}^{ee} is plotted against their kinetic energy (KE) for mono-energetic incident γ -rays of 1 MeV and 2.225 MeV. The kinetic energy of the recoiling electrons increases with E_{γ} as expected. The sharp right edge in the plots is the Compton edge. It is evident from Fig. 12 that a significant fraction of the electrons with higher recoil energies lose only ~ 280 keV of their energy within the detector. Therefore, we can conclude that the peak observed at higher channel numbers in the Fig. 6b corresponds to ~ 280 keV of E_{dep}^{ee} .

To further confirm this geometric effect, the simulation was repeated by changing the diameter of the fiducial volume of the detector to 30 mm and 90 mm. Corresponding E_{dep}^{ee} spectra are plotted in the Fig. 13. A clear shift in the peak can be seen, which is at ~ 130 keV for 30 mm diameter (solid line) and ~ 450 keV for 90 mm (dotted line).

Another systematic study was done to understand the effect of the SS cover of the detector. In this case, the SS cover was removed (keeping the original diameter of 60 mm unchanged for the active volume) and the corresponding E_{dep}^{ee} spectrum was obtained. It was observed that the height of the peak at ~ 280 keV had reduced in the spectrum indicating that the peak was, indeed, enhanced by the presence of the SS cover. The contribution from pair-production events to the RoI and in the overall spectra was evaluated from the E_{dep}^{ee} spectrum obtained after vetoing those events where pair-production has taken place. No significant deviation was observed from the spectrum of Fig. 11a, indicating that pair-production does not make significant

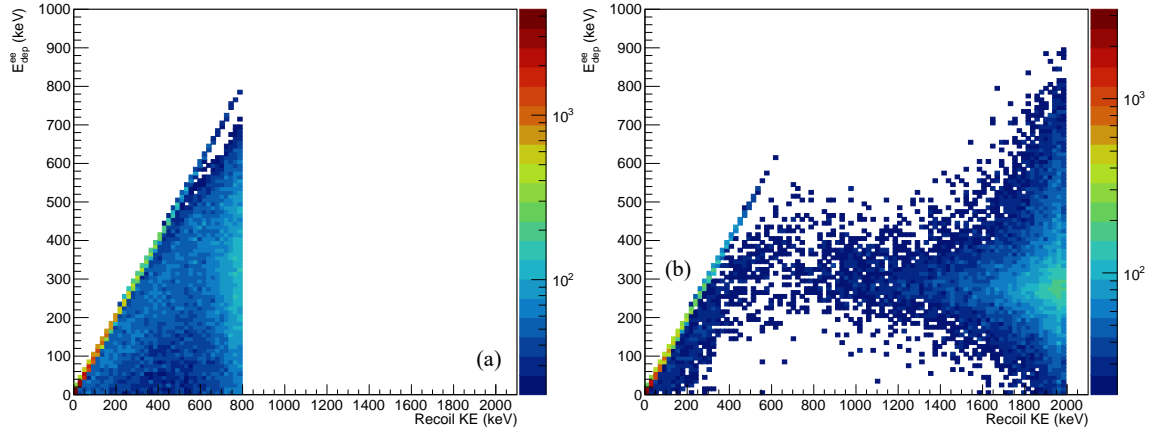


Figure 12: E_{dep}^{ee} vs. recoil kinetic energy of ER events from mono-energetic γ sources for (a) 1.0 MeV and (b) 2.22 MeV

contribution to the spectra. Additionally, it was observed from simulation that in almost all the cases, a single recoil electron is produced from a single γ -ray. The number of events with two recoil electrons from the incident γ -ray is almost two orders of magnitude lower than the single recoil events.

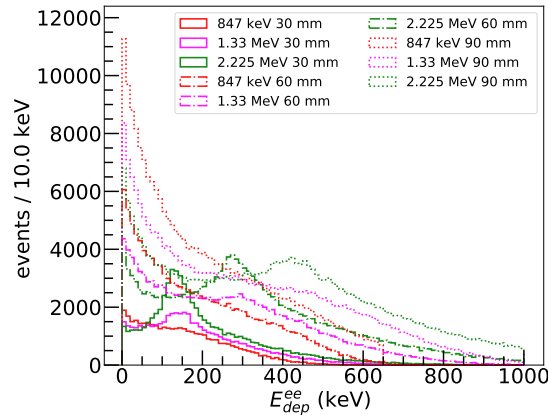


Figure 13: E_{dep}^{ee} spectra with 30 (solid lines), 60 (dot-dashed lines) and 90 mm (dotted lines) diameter of the SS housing.

Based on the experimental and the simulation results on the γ -ray response of the PHe detector, we can conclude that: 1) the $E_{dep}^{ee} \sim 280$ keV peak arising due to the most probable value of energy loss by the recoiling electrons within the confined geometry of the PHe detector. This is also seen as rising bump at the higher channel

numbers (~ 240) in the experiment (see Fig. 7b), apart from the spectral feature at the lower channel numbers (≤ 150) which has been demonstrated as arising from accompanying low energy γ -rays of the so-called room background. Based on the spectral profile of the E_{dep}^{ee} spectra, we fitted the peak with logistic function after subtracting an exponential background for the E_{dep}^{ee} spectra shown in the Fig. 11a, from 662 keV to 2.225 MeV γ -rays. The average E_{dep}^{ee} value for the peak was found to be: 282 ± 10 keV. Based on the above and the fact that the x -axis of the plots of the Fig. 7b scale as E_{dep}^{ee} , a first order calibration with calibration constant of 1.175 keV/channel on the x -axis is applied. 2) Observed attenuation of the low energy γ -rays by the HDPE layers, which is mostly due to scattering of the γ -rays, qualitatively agrees with the simulation. However, no quantitative comparison could be attempted in our study due to lack of information about the discrete γ -rays from the sources. 3) Production of the 2.225 MeV γ -rays and correlation with the attenuation of the fast neutrons by the HDPE layers have been found to demonstrate reasonable agreement between our experiment and the G4 simulation.

3.5. Neutron spectral calibration based on the neutron energy spectral data of ^{252}Cf

It is demonstrated through our G4 simulation that the ΔE values of the energy deposition by the neutrons inside the detector have a linear dependence of the neutron energy E_n (see Sec. 3.2 and Fig. 9b). Based on this observation, an alternative energy calibration of the detector was attempted using the prompt neutrons from a ^{252}Cf source. It is expected that the energy spectrum of the neutrons originating from the spontaneous fission is Maxwellian. However, after detailed analysis by various groups on the properties of neutron sources, and several meetings under the banner of International Atomic Energy Agency (IAEA), held during 1980 to 1987, the expert group on ^{252}Cf spontaneous fission-based fast neutron sources, had proposed a corrected Maxwellian spectrum, based on experimental data and theoretical estimates[17] over various energy segments from 0.2 MeV to 20 MeV. Accordingly, the corrected Maxwellian spectrum $F(E_n)$ as function of the kinetic energy (E_n) of the neutrons for the prompt fission neutrons is given by

$$F(E_n) = R(E_n) \frac{2}{\sqrt{\pi}} \frac{\sqrt{E_n}}{T^{3/2}} \exp\left[-\frac{E_n}{T}\right], \quad (1)$$

where, $R(E_n)$ is the proposed correction factor to the Maxwellian spectrum, and T is the nuclear temperature of ^{252}Cf before fission, with typical value of 1.42 MeV[17]. Based on Mannhart's correction factors, a least squares-fitted polynomial regression model was introduced in the Los Alamos ORNL MCNP-DSP code [18]. The $R(E_n)$ values, based on the above, were used to obtain the corrected Maxwellian form for the

^{252}Cf prompt neutrons to arrive at the benchmark ^{252}Cf prompt neutron spectrum. Finally, the simulated spectrum was folded by the intrinsic detector efficiency data available from Ref. [19] by applying cubic spline interpolation. It may be noted that the intrinsic efficiency data, obtained from the time of flight (TOF) measurements, is available in the range of 0.5 MeV to 6.5 MeV, with backward interpolation extended to 0.35 MeV.

The measured and the simulated efficiency values given in Ref. [19] considerably differ over various energy ranges. Therefore, the experimentally obtained spectrum was compared with the theoretical one after folding the latter with: 1) the experimentally obtained efficiencies $\epsilon_{\text{ex}}(E_n)$, 2) simulated efficiencies $\epsilon_{\text{th}}(E_n)$, and 3) average of the two efficiencies as mentioned above, estimated at each energy. Our comparisons reveal the best match for the $\epsilon_{\text{ex}}(E_n)$, which is shown in the Fig. 14. It is evident that the lower energy part of the spectrum reveals a cut-off around 0.75 MeV, which is possibly contributed by the threshold discriminator setting and also the merging threshold of the neutron and the γ -bands in our experiment (refer to Fig. 2).

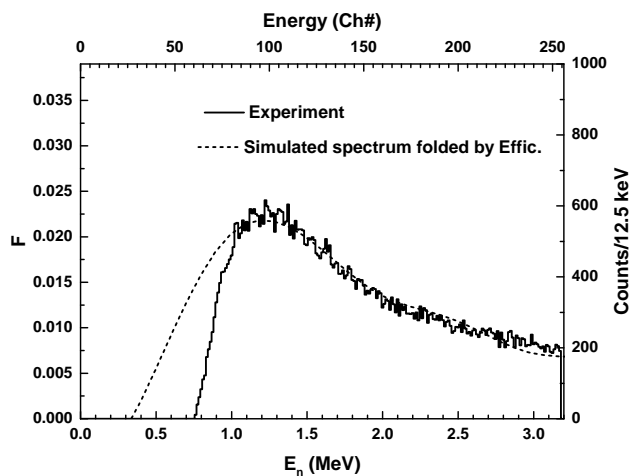


Figure 14: Overlaid experimental and theoretically estimated energy spectra of neutrons from the ^{252}Cf spontaneous fission source. The top axis label displays the QDC channel number and the bottom axis labels are the energy of the neutrons.

A comparison of the experimentally obtained ^{252}Cf prompt neutron spectrum and the one theoretically obtained as above, are shown in the Fig. 14. They are found to be in good agreement over the energy range of 0.7 MeV to 3.2 MeV. It is important to mention two major points here. a) The upper limit of the available energy range is due to the gain settings of the built-in amplifiers associated with the ^4He detector. b) Our comparison, shown in the Fig. 14, manifests that the measured spectrum

is constrained by a lower energy cut-off around 0.75 MeV, whereas the estimated spectrum, folded by the efficiency data, has a lower energy cut-off of around 0.35 MeV which arises entirely from the available intrinsic efficiency data in Ref. [19].

There are uncertainties in this method of calibration, which is primarily caused by the sparse data on the intrinsic efficiency. The measured and the simulated efficiency results considerably differ over various energy ranges[19]. Besides, interpolation procedure followed leaves scope for introducing additional uncertainties. Because of these uncertainties, we have adopted a linear calibration without a cut-off. However, a least square fit of the calibration data up to the quadratic term (ie. $E_n(x) = a_0 + a_1x + a_2x^2$, where x is the channel number), results in the following best fit values: $a_0 = 0.00167 \pm 0.00212$ MeV, $a_1 = 0.0125 \pm 3.93 \times 10^{-5}$ MeV/ch, $a_2 = 1.87 \times 10^{-8} \pm 1.48 \times 10^{-7}$ MeV/ch². Relatively smaller values of a_0 and a_2 justify our choice of linear calibration.

It may be noted that the detector is also capable of detecting the γ -rays due to its electron recoil response, though the intrinsic detection efficiency may be very small compared to that of the neutrons. Though considerable details about the shape of the energy spectral distribution of γ -rays from spontaneous fission of ²⁵²Cf is available[20], similar energy calibration procedure could not be attempted for the γ -ray spectra, because of the overlap of the neutron and the γ -bands (see Fig. 2) at lower energies.

4. Scintillation signal estimates for the PHe detector

In our simulation work, we have so far followed the transfer of energy from the radiation quanta (neutrons or γ -rays) to the recoiling medium particles (⁴He or electron). There are primarily three mechanisms by which, a recoiling ⁴He (NR events) loses its energy along its track, viz. ionization, charge-exchange collisions and excitation collisions. The cross-sections of these interactions depend on the charge-state of the recoiling ⁴He itself. Electron-ion pairs are produced by ionization. While in charge-exchange collisions, ions are generated through electron-capture interactions by the recoiling He¹⁺ and He²⁺ ions. Conversely, free electrons are produced from He⁰ and He¹⁺ ions through the loss of electrons. When these electron-ion pairs recombine, Helium excimer states are formed. Additionally, they are also formed when excited He-atoms resulting from excitation collisions, combine with ground state He-atoms. Therefore, one of the main outcomes of these interactions is the formation of the Helium excimer molecules. These excimer molecules can be in spin-singlet or spin-triplet states (their proportion dependent on the production mechanism). The spin-singlet states decay promptly via radiative transitions and give rise to prompt

scintillation, which is termed as the S1 signal, whereas the spin-triplet states are long-lived but they too decay radiatively and contribute to the delayed S3 signal[21].

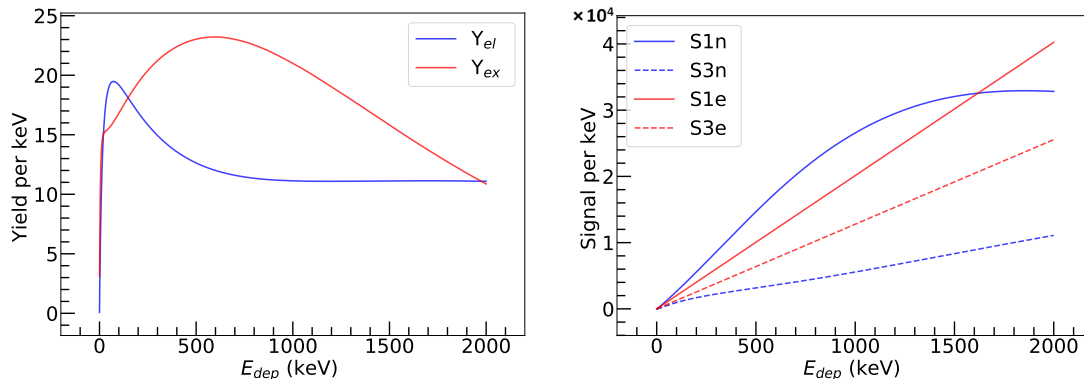


Figure 15: (a) Yield vs. recoil energy of ${}^4\text{He}$. The e^- -ion pair yield is shown in blue and excitation yield is shown in red; (b) S1 and S3 signal intensities vs. recoil energy for NR (red) and ER (blue) events in pressurized ${}^4\text{He}$.

The above mechanism also works for the ER events, except for the absence of charge-exchange collisions. From the discussion, it can be concluded that the determining parameter for the intensity of these signals is the number of electron-ion pairs and excitation produced for a given recoil energy. The calculation of the yield (number per unit recoil energy) and the signal intensities have been worked out in detail [21]. The density of helium-4 gas at 180 bar pressure and 300 K temperature is taken as $0.0247 \text{ g} \cdot \text{cm}^{-3}$ and the number density is $3.7 \times 10^{21} \text{ cm}^{-3}$. Figure 15a shows the yield vs. recoil energy of ${}^4\text{He}$, where the blue curve is the electron-ion ionization yield and the red curve is the excitation yield. The ionization and excitation yields due to ER are considered constant at 22.7 keV^{-1} and 10.2 keV^{-1} respectively [21]. Figure 15b depicts the S1 and S3 signal intensities as a function of the recoil energy. The blue and the red curves represent NR and ER events respectively. The plot of the S1 signal distribution for NR and ER events for incident neutrons is shown in Fig. 16a and Fig. 16b respectively for different number of the HDPE layers placed in between. The incident energy of the neutrons is sampled from the energy distribution obtained from the ${}^{11}\text{B}(\alpha, n){}^{14}\text{N}$ reaction (see Fig. 7). The γ -rays produced from the ${}^{241}\text{Am}$ source and also due to interaction of the source neutrons with the intervening media have been taken into account for the S1-S3 signal estimates.

We have plotted the events on the S1-S3 plane for incident neutrons to estimate the bands corresponding to NR and ER events. This is shown in the Fig. 17. Here the narrow band towards the left side is due to the ER events (from the γ -rays

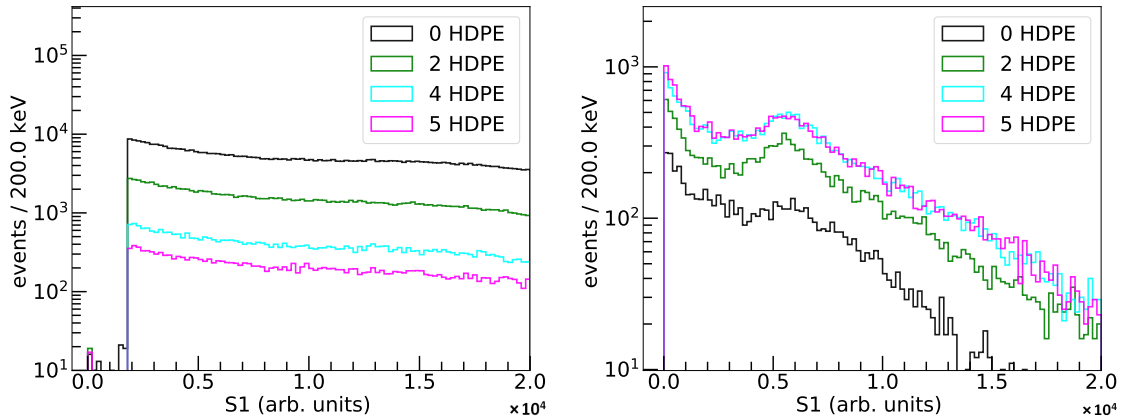


Figure 16: S1 signal distribution for (a) NR events, and (b) ER events.

produced in the nuclear reactions), while the band towards the right side is due to the NR events. In the NR band, most of the events cluster within a curve-like region (indicated by red). This is a consequence of saturation of the S1 signal at larger recoil energies of ^4He , as illustrated in the Fig. 15b.

Based on the above simulations, we can conclude that by combining the S1 and S3 scintillation signals arising from the fast and the slow decay of the $^4\text{He}^*_2$ excimer states, a discrimination between NR and the ER events can be done. Our present simulation-based study does not have a scope to estimate the realistic background which can constrain the above threshold. Unusually long decay time ($\sim 13\text{s}$) of the triplet state leading to the S3 signal may also severely limit the suitability of the proposed method.

5. Conclusion

Pressurized ^4He detector, capable of detecting and discriminating between the neutrons and the γ -rays in a mixed radiation field, has been evaluated in detail both through source-based experiment and G4-based simulation.

The experimental studies based on ^{252}Cf fast neutron source, ^{137}Cs γ -reference source and ^{241}Am source have successfully demonstrated that a fast and a slow gate-based integration of the detector output pulses by the QDC is effective in achieving discrimination. Attenuation of the neutron band by the HDPE layers placed between the source and the detector also confirms the discrimination method followed. The charge contents of the pulses over the long gate effectively scale as the energy deposited E_{dep} by the recoiling ^4He in case of the neutrons, or the recoiling electrons in case of the γ -rays. Based on the estimated fast neutron energy spectrum arising

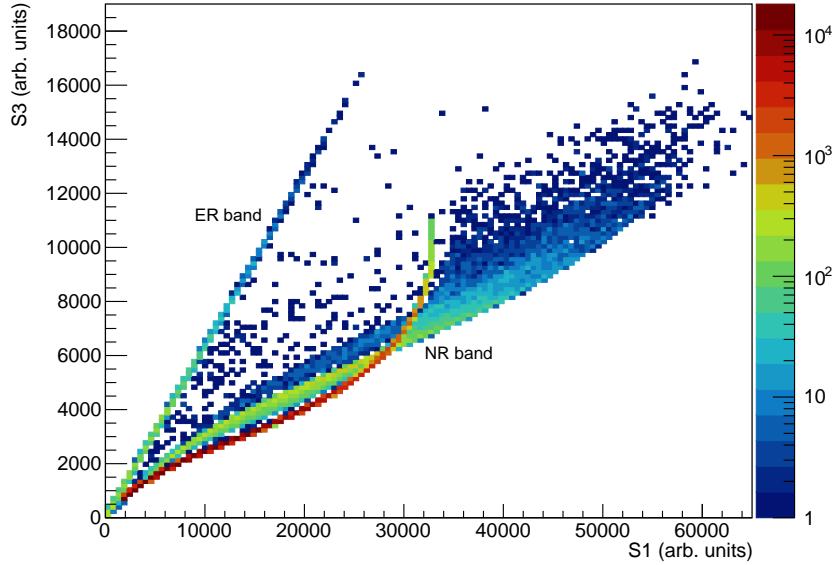


Figure 17: S3 vs. S1 for NR and ER events due to the incident neutrons.

from the spontaneous fission of ^{252}Cf [17], and the PHe detector efficiency data[19] for the fast neutrons, the measured E_{dep} spectral profile has been found to match reasonably well with theoretically estimated profile, folded by the detector efficiency. The lower energy part of the spectral profile, however, do not match due to the difference in the threshold for our measurement and the PHe detector efficiency data, which was based on the time-of-flight measurements[19]. The measured spectral distribution was calibrated over a range in terms of the neutron energy, based on the above match of the profiles. The same calibration was applied for the measured neutron spectra pertaining to the ^{241}Am source based measurements.

Parallel measurement of the γ -ray spectral profiles for the radioactive sources mentioned above were also done. The γ -ray spectra, arising due to the scintillation caused by the corresponding electron recoil events, reveal peak-like structures at the larger E_{dep} values, which is grossly correlated with the placement of HDPE absorbers between the source and the detector.

Interaction of the neutrons and the γ -rays with the HDPE layers was investigated in detail through Geant4 based simulation. Production of the neutrons from the ^{241}Am source was demonstrated to be largely due to the (α, n) reactions on the constituent elements of the glass substrate. Corresponding neutron spectrum was used for the event generation. Neutron attenuation by the HDPE layers was successfully reproduced to qualitatively match with the experimental results. Interaction

of the γ -rays emitted from the ^{241}Am source and also produced through neutron absorption by the HDPE layers with the pressurized helium active medium, were studied to find the origin of the peak-like structures in the measured spectra. It is found that a significant number of relatively higher energy γ -rays ($E_\gamma \gtrsim 650$ keV) produce recoiling electrons, which dump around 280 keV of energy, resulting in the peak-like structure. Role of the SS housing of the detector and its geometry were also investigated as part of the systematic studies in support of the above.

The scintillation signals from the pressurized ^4He has been estimated following the formalism of Guo and McKinsey[21]. Estimation of the S1 and S3 signals due to scintillation were worked out. We have demonstrated that a combination of the (S1,S3) signal can be used as a potential method to discriminate between the neutrons and the γ -rays. It may be useful for a future dark matter direct search experiment, provided a very low threshold on the NR-ER discrimination can be achieved. Alternatively, a time projection chamber (TPC) based on pressurized ^4He as the active medium, should be investigated where the possibility of discrimination using the scintillation (S1) and the ionization (S2) signals may be explored. As mentioned before, relatively smaller number of available electrons make the PHe detector much less sensitive to the γ -ray / electron recoil background.

We have estimated the sensitivity limit of a suitable pressurized ^4He detector (either as a scintillator or a TPC) if it can be configured and deployed as a detector in search of dark matter candidates. Considering low mass WIMPs as a suitable dark matter candidate, the exclusion limit is estimated assuming zero background, which makes this an ideal scenario. Given that ^4He has a mass of about 77 kg when filled inside a 1 metre diameter \times 1 metre long barrel at 180 bar pressure, the total exposure for a year-long physics run amounts to 77 kg \cdot year. The WIMP-nucleon cross-section is calculated following the method described by Lewin and Smith [22] for the spin-independent case. It assumes a Maxwellian distribution for the velocity of WIMP having 220 km \cdot s $^{-1}$ as the most probable value. The mean WIMP density is estimated at 0.4 GeV \cdot c 2 \cdot cm $^{-3}$ [22]. The recoil energy range is taken as 0.5 - 100 keV. The upper limit at 90% CL on the expected signal is determined to be 2.44 in the absence of any observation using the Feldman-Cousins method [23]. This gives an expected event rate of 0.032 kg $^{-1}$ year $^{-1}$ for 77 kg \cdot year exposure. The corresponding projected sensitivity limit is depicted in Fig. 18. The experiment will be optimally sensitive to rule out the existence of WIMP having mass ~ 3.5 GeV \cdot c $^{-2}$ at 3.5×10^{-44} cm 2 cross-section level. Obviously, this is an ideal situation which will be constrained due to the presence of background to push the projected sensitivity limit up further.

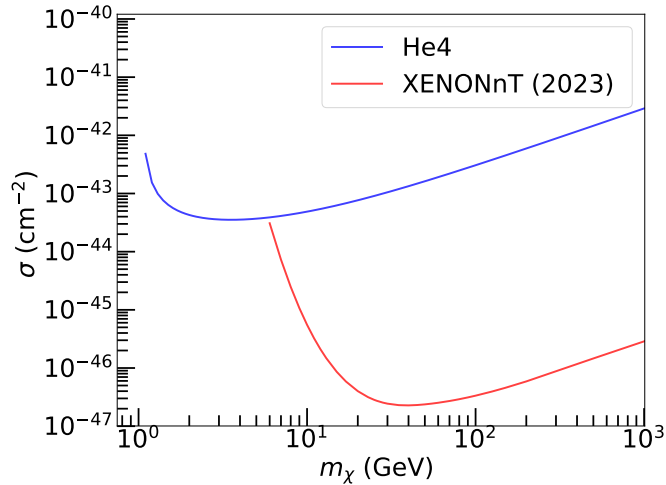


Figure 18: Projected sensitivity limit at 90% CL with no background; XENONnT upper limit at 90% CL (2023) result for reference [24]

6. Acknowledgements

We are grateful to Prof. Satyaki Bhattacharya of SINP, India, for the invaluable discussions on the statistical analysis for the sensitivity calculation. We would also like to acknowledge technical and operational support from Chandranath Marick of SINP, India. One of us (SS) would like to acknowledge financial support from the Department of Atomic Energy Raja Ramanna Fellowship (DAE-RRF) scheme to carry out this work.

References

- [1] R. C. Runkle, A. Bernstein, P. E. Vanier, Securing special nuclear material: Recent advances in neutron detection and their role in nonproliferation, *Jour. App. Phys.* 108 (2012) 111101. [doi:10.1063/1.3503495](https://doi.org/10.1063/1.3503495).
- [2] S. Ghosh, S. Dutta, N. K. Mondal, S. Saha, Measurements of gamma ray, cosmic muon and residual neutron background fluxes for rare event search experiments at an underground laboratory, *Astropart. Phys.* 139 (2022) 102700. [doi:10.1016/j.astropartphys.2022.102700](https://doi.org/10.1016/j.astropartphys.2022.102700).
- [3] E. H. Thorndike, W. J. Shlaer, Scintillations from Liquid Helium, *Rev. Sci. Instrum.* 30 (1959) 838. [doi:10.1063/1.1716775](https://doi.org/10.1063/1.1716775).

- [4] R. Chandra, G. Davatz, H. Friederich, U. Gendottia, D. Murer, Fast neutron detection with pressurized ^4He scintillation detectors, *Jour. Instrum.* 7 (2012) C03035. doi:[10.1088/1748-0221/7/03/C03035](https://doi.org/10.1088/1748-0221/7/03/C03035).
- [5] R. Kelley, D. Murer, D. Ray, K. Jordan, Analysis of the scintillation mechanism in a pressurized ^4He fast neutron detector using pulse shape fitting, *AIP Advances* 5 (2015) 037144. doi:[10.1063/1.4916904](https://doi.org/10.1063/1.4916904).
- [6] D. Murer, He-4 Fast Neutron Detectors in Nuclear Security Applications, Ph.D. thesis, ETH Zurich (2014). doi:[10.3929/ethz-a-010111172](https://doi.org/10.3929/ethz-a-010111172).
- [7] R. Jebali, A first comparison of the responses of a ^4He -based fast-neutron detector and a NE-213 liquid-scintillator reference detector, *Nucl. Instrum. Meth. A* 794 (2015) 102. doi:<http://dx.doi.org/10.1016/j.nima.2015.04.058>.
- [8] Arktis Radiation Detectors Limited, Zurich, Switzerland, Arktis s670e detector series operating manual, https://www.arktis-detectors.com/fileadmin/user_upload/ARK-S670e-FTND-0818.pdf (2017).
- [9] O. Searfus, K. Ogren, I. Jovanovic, Digital pulse analysis for fast neutron recoil spectroscopy with a ^4He scintillation detector, *Nucl. Instrum. Meth. A* 1046 (2023) 167703. doi:[10.1016/j.nima.2022.167703](https://doi.org/10.1016/j.nima.2022.167703).
- [10] H. Friederich, Development of a Readout System for Noble Gas Detectors, Ph.D. thesis, ETH Zurich (2013). doi:[10.3929/ethz-a-010055270](https://doi.org/10.3929/ethz-a-010055270).
- [11] M. W. Watson, R. Venkataraman, S. Croft, Characterization of ^{252}Cf sources using high-resolution gamma spectroscopy, *Applied Radiation and Isotopes* 169 (2021) 109531. doi:<https://doi.org/10.1016/j.apradiso.2020.109531>.
- [12] S. Agostinelli, J. Allison, K. Amako, J. Apostolakis, H. Araujo, P. Arce, M. Asai, D. Axen, S. Banerjee, G. Barrand, F. Behner, L. Bellagamba, J. Boudreau, L. Broglia, A. Brunengo, H. Burkhardt, S. Chauvie, J. Chuma, R. Chytracsek, G. Cooperman, G. Cosmo, P. Degtyarenko, A. Dell'Acqua, G. Depaola, D. Dietrich, R. Enami, A. Feliciello, C. Ferguson, H. Fesefeldt, G. Folger, F. Foppiano, A. Forti, S. Garelli, S. Giani, R. Giannitrapani, D. Gibin, J. Gómez Cadenas, I. González, G. Gracia Abril, G. Greeniaus, W. Greiner, V. Grichine, A. Grossheim, S. Guatelli, P. Gumplinger, R. Hamatsu, K. Hashimoto, H. Hasui, A. Heikkinen, A. Howard, V. Ivanchenko, A. Johnson, F. Jones, J. Kallenbach, N. Kanaya, M. Kawabata, Y. Kawabata, M. Kawaguti, S. Kellner, P. Kent, A. Kimura, T. Kodama, R. Kokoulin, M. Kossov, H. Kurashige,

- E. Lamanna, T. Lampén, V. Lara, V. Lefebure, F. Lei, M. Liendl, W. Lockman, F. Longo, S. Magni, M. Maire, E. Medernach, K. Minamimoto, P. Mora de Freitas, Y. Morita, K. Murakami, M. Nagamatu, R. Nartallo, P. Nieminen, T. Nishimura, K. Ohtsubo, M. Okamura, S. O’Neale, Y. Oohata, K. Paech, J. Perl, A. Pfeiffer, M. Pia, F. Ranjard, A. Rybin, S. Sadilov, E. Di Salvo, G. Santin, T. Sasaki, N. Savvas, Y. Sawada, S. Scherer, S. Sei, V. Sirotenko, D. Smith, N. Starkov, H. Stoecker, J. Sulkimo, M. Takahata, S. Tanaka, E. Tcherniaev, E. Safai Tehrani, M. Tropeano, P. Truscott, H. Uno, L. Urban, P. Urban, M. Verderi, A. Walkden, W. Wander, H. Weber, J. Wellisch, T. Wenaus, D. Williams, D. Wright, T. Yamada, H. Yoshida, D. Zschesche, [Geant4—a simulation toolkit](#), Nucl. Instrum. Meth. A 506 (3) (2003) 250–303. doi:[https://doi.org/10.1016/S0168-9002\(03\)01368-8](https://doi.org/10.1016/S0168-9002(03)01368-8).
URL <https://www.sciencedirect.com/science/article/pii/S0168900203013688>
- [13] E. Mendoza, D. Cano-Ott, P. Romojaro, V. Alcayne, P. García Abia, V. Pesudo, L. Romero, R. Santorelli, [Neutron production induced by alpha-decay with geant4](#), Nucl. Instrum. Meth. A 960 (2020) 163659. doi:<https://doi.org/10.1016/j.nima.2020.163659>.
URL <https://www.sciencedirect.com/science/article/pii/S0168900220302333>
- [14] J. Tuli, [Evaluated nuclear structure data file](#), Nucl. Instrum. Meth. A 369 (2) (1996) 506–510. doi:[https://doi.org/10.1016/S0168-9002\(96\)80040-4](https://doi.org/10.1016/S0168-9002(96)80040-4).
URL <https://www.sciencedirect.com/science/article/pii/S0168900296800404>
- [15] A. Trkov, D. A. Brown, [Endf-6 formats manual: Data formats and procedures for the evaluated nuclear data files](#) (1 2018). doi:[10.2172/1425114](https://doi.org/10.2172/1425114).
URL <https://www.osti.gov/biblio/1425114>
- [16] T. Murata, H. Matsunobu, K. Shibata, Evaluation of the (α , xn) reaction data for JENDL/AN-2005 (2006).
- [17] W. Mannhart, [Evaluation of the Cf-252 fission neutron spectrum between 0 MeV and 20 MeV](#) IAEA TECDOC-410 (1987) 158–171.
URL https://inis.iaea.org/collection/NCLCollectionStore/_Public/18/076/18076628.pdf
- [18] T. E. Valentine, [MCNP-DSP USERS MANUAL](#) (2001). doi:[10.2172/777654](https://doi.org/10.2172/777654).
URL <https://www.osti.gov/biblio/777654>

- [19] Y. Liang, T. Zhu, C. E. Parker, A. L. Richard, T. N. Massey, R. Chandra, H. Ray, K. A. Jordan, J. Baciak, A. Enqvist, [Neutron spectroscopy and spectral unfolding with a \$^4\text{He}\$ fast neutron scintillators](#), Nuclear Instruments and Methods in Physics Research Section A: Accelerators, Spectrometers, Detectors and Associated Equipment 922 (2019) 1–7. doi:<https://doi.org/10.1016/j.nima.2018.10.098>.
URL <https://www.sciencedirect.com/science/article/pii/S0168900218314128>
- [20] J. M. Verbeke, C. Hagmann, D. Wright, [Simulation of Neutron and Gamma Ray Emission from Fission and Photofission](#). LLNL Fission Library 2.0.2 UCRL-AR-228518-REV-1 (2016).
URL <https://nuclear.llnl.gov/simulation/fission.pdf>
- [21] W. Guo, D. N. McKinsey, [Concept for a dark matter detector using liquid helium-4](#), Phys. Rev. D 87 (2013) 115001. doi:[10.1103/PhysRevD.87.115001](https://doi.org/10.1103/PhysRevD.87.115001).
URL <https://link.aps.org/doi/10.1103/PhysRevD.87.115001>
- [22] J. Lewin, P. Smith, [Review of mathematics, numerical factors, and corrections for dark matter experiments based on elastic nuclear recoil](#), Astroparticle Physics 6 (1) (1996) 87–112. doi:[https://doi.org/10.1016/S0927-6505\(96\)00047-3](https://doi.org/10.1016/S0927-6505(96)00047-3).
URL <https://www.sciencedirect.com/science/article/pii/S0927650596000473>
- [23] G. J. Feldman, R. D. Cousins, [Unified approach to the classical statistical analysis of small signals](#), Phys. Rev. D 57 (1998) 3873–3889. doi:[10.1103/PhysRevD.57.3873](https://doi.org/10.1103/PhysRevD.57.3873).
URL <https://link.aps.org/doi/10.1103/PhysRevD.57.3873>
- [24] E. Aprile, K. Abe, F. Agostini, S. Ahmed Maouloud, L. Althueser, B. Andrieu, E. Angelino, J. R. Angevaere, V. C. Antochi, D. Antón Martín, F. Arneodo, L. Baudis, A. L. Baxter, M. Bazyk, L. Bellagamba, R. Biondi, A. Bismark, E. J. Brookes, A. Brown, S. Bruenner, G. Bruno, R. Budnik, T. K. Bui, C. Cai, J. M. R. Cardoso, D. Cichon, A. P. Cimental Chavez, A. P. Colijn, J. Conrad, J. J. Cuenca-García, J. P. Cussonneau, V. D’Andrea, M. P. Decowski, P. Di Gangi, S. Di Pede, S. Diglio, K. Eitel, A. Elykov, S. Farrell, A. D. Ferella, C. Ferrari, H. Fischer, M. Flierman, W. Fulgione, C. Fuselli, P. Gaemers, R. Gaior, A. Gallo Rosso, M. Galloway, F. Gao, R. Glade-Beucke, L. Grandi, J. Grigat, H. Guan, M. Guida, R. Hamann, A. Higuera, C. Hils,

L. Hoetsch, N. F. Hood, J. Howlett, M. Iacovacci, Y. Itow, J. Jakob, F. Joerg, A. Joy, N. Kato, M. Kara, P. Kavargin, S. Kazama, M. Kobayashi, G. Koltman, A. Kopec, F. Kuger, H. Landsman, R. F. Lang, L. Levinson, I. Li, S. Li, S. Liang, S. Lindemann, M. Lindner, K. Liu, J. Loizeau, F. Lombardi, J. Long, J. A. M. Lopes, Y. Ma, C. Macolino, J. Mahlstedt, A. Mancuso, L. Manenti, F. Marignetti, T. Marrodán Undagoitia, K. Martens, J. Masbou, D. Masson, E. Masson, S. Mastroianni, M. Messina, K. Miuchi, K. Mizukoshi, A. Molinaro, S. Moriyama, K. Morá, Y. Mosbacher, M. Murra, J. Müller, K. Ni, U. Oberlack, B. Paetsch, J. Palacio, R. Peres, C. Peters, J. Pienaar, M. Pierre, V. Pizzella, G. Plante, J. Qi, J. Qin, D. Ramírez García, R. Singh, L. Sanchez, J. M. F. dos Santos, I. Sarnoff, G. Sartorelli, J. Schreiner, D. Schulte, P. Schulte, H. Schulze Eißing, M. Schumann, L. Scotto Lavina, M. Selvi, F. Semeria, P. Shagin, S. Shi, E. Shockley, M. Silva, H. Simgen, A. Takeda, P.-L. Tan, A. Terliuk, D. Thers, F. Toschi, G. Trincherro, C. Tunnell, F. Tönnies, K. Valerius, G. Volta, C. Weinheimer, M. Weiss, D. Wenz, C. Wittweg, T. Wolf, V. H. S. Wu, Y. Xing, D. Xu, Z. Xu, M. Yamashita, L. Yang, J. Ye, L. Yuan, G. Zavattini, M. Zhong, T. Zhu, [First dark matter search with nuclear recoils from the xenonnT experiment](#), Phys. Rev. Lett. 131 (2023) 041003. doi:[10.1103/PhysRevLett.131.041003](https://doi.org/10.1103/PhysRevLett.131.041003).
URL <https://link.aps.org/doi/10.1103/PhysRevLett.131.041003>